Available online at www.sciencedirect.com

SCIENCE DIRECT

Cement and Concrete Research 35 (2005) 67–75

CEMENT AND CONCRETE RESEARCH

Mechanical approach in mitigating alkali-silica reaction

C.K. Yi, C.P. Ostertag*

Civil and Environmental Engineering Department, University of California, Berkeley, CA 94720, USA

Received 9 July 2003; accepted 20 February 2004

Abstract

The effect of steel microfibers (SMF) on alkali-silica reaction (ASR) was investigated using two types of reactive aggregates, crushed opal and a Pyrex rod of constant diameter. Cracks are less visible in the SMF mortars compared with the unreinforced mortars. Due to crack growth resistance behavior in SMF mortar specimens, the strength loss is eliminated and the ASR products remained well confined within the ASR site. The expansion and the ASR products were characterized by microprobe analysis and inductive coupled plasma (ICP) spectroscopy. The confinement due to SMF resulted in a higher Na and Si ion concentration of the ASR liquid extracted from the reaction site. The higher concentration reduced the ASR rate and resulted in a lower reactivity of the reactive Pyrex rods in SMF mortars.

Keywords: Alkali-aggregate reaction; Microcracking; Expansion; Tensile properties; Fiber reinforcement

1. Introduction

The reaction between alkalis from cement and certain forms of silica present in aggregates is called alkali-silica reaction (ASR). Hydroxide ions attack the Si-O bond of the silica present in aggregates, creating an alkali-silica gel that is capable of swelling by imbibing water. The resulting volumetric expansion causes cracking and can lead to strength and stiffness reduction in concrete structures. Damage associated with ASR can be avoided by preventing the expansion or the formation of the ASR gel. This may be accomplished through either a chemical or a mechanical approach. The latter physically restrains the expansion of the alkali-silica gel [1–5]. However, most of the research focuses on the chemical approach by modifying the chemical environment in which the ASR takes place through mineral admixtures [6–9] or addition of lithium salts [10,11]. In many cases, influencing the reaction chemistry proved to be effective in reducing the expansion and hence damage associated with ASR. However, sometimes the results are contradictory not only due to the wide varieties of reactive aggregate types and sizes and cement types but also due to variations in chemical compositions [12] and agglomerations [13,14] of mineral admixtures and due to differences in lithium salt additions [15].

This article reports on mitigating ASR through a mechanical approach that focuses on reducing the cracking and ASR gel expansion through steel microfiber (SMF) reinforcements. Because cracks due to ASR start as microcracks, microfibers were chosen over macrofibers to control these microcracks at onset. Furthermore, microfibers are very effective in providing crack control through toughening mechanisms that promote crack growth resistance behavior [16]. The effect of crack growth resistance on expansion and ASR gel formation will be discussed.

The effect of SMFs on ASR was investigated using two different types of reactive aggregates. The cracking, strength and expansion characteristics due to SMFs were determined using crushed opal aggregates. The influence of microfibers on reactivity, gel formation and gel composition was investigated using a rod-shaped reactive Pyrex aggregate of constant diameter. For this type of study, the opal aggregates with their irregular shapes and sizes are not well suited. This novel method of using the rod-shaped aggregate of constant diameter also lends itself to determine the solid and liquid reaction products associated with ASR in detail.

* Corresponding author. Tel.: +1-510-642-0184; fax: +1-510-643-8928.
E-mail address: ostertag@ce.berkeley.edu (C.P. Ostertag).

0008-8846/$ – see front matter © 2004 Elsevier Ltd. All rights reserved.
doi:10.1016/j.cemconres.2004.02.017

2. Experimental procedure

2.1. Crushed opal as reactive aggregate

The following experiments were conducted with crushed opal aggregates: (a) microscopy analysis on cracking due to ASR, (b) crack propagation tests to measure the deterioration of the mechanical properties due to ASR and (c) expansion experiments according to ASTM C-1260 [17]. For these experiments, the SMF content was either 0 or 7 vol.%. The rectangular cross-section and length of the SMFs are 20×100 μm and 3–5 mm, respectively. Mortar bars used for the ASR expansion experiment were made according to ASTM C-1260 [17] using type I/II Portland cement and graded fine aggregates. The total amount of opal constituted 5% of the total fine aggregates by mass. The mix proportions for the specimens are given in Table 1. The test was modified by adding 5 days of underwater curing at 80 °C (7 days of total curing) before submerging the specimens in aqueous 1 N NaOH solution. Additional curing was shown by Turanli et al. [18] to increase the bond strength between the fibers and the cement paste matrix, thereby increasing their effectiveness in controlling expansion.

Strength properties of the specimens ($2.5 \times 2.5 \times 28.58$ cm) with and without SMFs were measured in third point loading after they were exposed to the NaOH solution for 0, 7 and 14 days. Three beams were tested for each exposure time. For the crack propagation measurements, compact tension specimens ($5 \times 5 \times 6$ mm) were tested after exposure to the NaOH solution for 0, 7 and 14 days. Three specimens were tested for each exposure time. Detailed information on the loading device and testing procedure can be found in Ostertag and Yi [19].

2.2. Pyrex rod as reactive aggregate

Unreinforced and SMF reinforced specimens with a Pyrex rod (5.27 ± 0.01 mm in diameter) as the reactive aggregate embedded in their center were used (a) to determine the difference in reactivity of the reactive aggregates in the presence of a SMF reinforced matrix, (b) for microprobe analysis to reveal and determine the chemical composition of the solid ASR and (c) for inductive coupled plasma (ICP) spectroscopy to determine the composition of the liquid alkali-silica complex.

Two sets of short prisms, $24.5 \times 24.5 \times 73.5$ mm ($1 \times 1 \times 3$ in.) with and without SMFs, were prepared using Pyrex rods (5.27 ± 0.01 mm in diameter). The mortar mix proportions were the same as above, except for the opal aggregates. The mortar (with 0 and 7 vol.% of SMFs) was placed in two layers, each layer with ~ 12 mm (0.5 in.) in thickness. The rod was placed in the center of the specimen between the two layers. The same curing schedule was applied as in Section 2.1.

The reactivity of the Pyrex rod due to ASR in the control and microfiber reinforced mortars was determined by measuring the remaining diameter of the Pyrex rod after it had been exposed to the alkali solution for up to 77 days. The prisms from each set were removed from the NaOH solution at intervals of 7–8 days.

Microprobe analysis was performed on the rods to analyze the chemical composition of the gel and the surrounding cement paste. For the microprobe analysis, thin sections of mortar specimens with smooth surfaces had to be prepared. The specimens were cut in the center and dried in the desiccators and the cut surface was embedded in epoxy. The epoxy was poured in vacuum to avoid possible air bubbles. The epoxy is cured at room temperature for 3 days instead of quick oven drying to minimize thermal mismatch between epoxy and cement paste. The face with the epoxy coating was then polished with Al-carbide grit of size 600 and a glass plate was glued to the surface using UV activated cement. The sample is then cut close to the glass plate such that the thickness of the sample is about 30 μm. The sample is further polished with polishing grits (9 and 3 μm) and paste (0.25 μm), respectively. Throughout the polishing process, kerosene was used as the fluid medium to minimize disturbance in water-sensitive hydrated cement samples.

The liquid phase of the ASR product near the Pyrex rod was collected from the prisms prepared in the same manner as described above with one variation, the length of the prisms. A 9 in. long Pyrex rod was embedded in the center of $10 \times 1 \times 1$ in. prism made of mortar with or without SMFs. Some specimens were exposed to the 1 N NaOH solution up to 80 days. In preparation for the liquid extraction, both ends of the prism were first saw cut to create a notch deep enough to be broken off by hand. This procedure was done to prevent the liquid ASR products to be contaminated by the external water used as coolant. The specimens were dried in the air before removing the ends. The prism without ends was held vertically and a low air pressure was applied at one end to increase the flow of the liquid. The liquid ASR products were then collected in airtight plastic tubes and the chemical composition of the

Table 1
Mix proportions for ASR expansion test

	Control	7 vol.% steel fiber
Cement (g)	440	440
Water (ml)	206.8	206.8
Aggregate (g)	990.0	854.4
SMF (g)	0.0	404.6

Detailed aggregate size distribution

Sieve no.	Control		7 vol.% steel fiber	
	Sand (g)	Opal (g)	Sand (g)	Opal (g)
8	94.05	4.95	81.17	4.27
16	235.13	12.37	202.92	10.68
30	235.13	12.37	202.92	10.68
50	235.13	12.37	202.52	10.68
100	141.08	7.42	121.76	6.4
	990.0		854.4	

liquids was obtained from the mortars with and without SMF analyses by ICP spectrometry.

3. Results

3.1. Crushed opal as reactive aggregate

3.1.1. Cracking characteristics

Polished surfaces were examined to investigate any changes in morphology of the mortar and opal aggregates. Fig. 1 show a typical opal aggregate after it has reacted with alkalis. The reaction product is recognized by the rim formation. The opal aggregate can easily be removed during the polishing process, leaving a hollow cavity behind. A microcrack has formed in the unreinforced mortar specimen due to the ASR. The crack is filled with a gel substance, similar in texture as the silica gel observed in the reaction rim. The silica gel in the microcracks can exert stresses on the crack faces causing widening of the crack and rapid deterioration of the matrix before absorbing large amount of Ca^{2+} ions from the cement paste. Therefore, the ability for the extruded gel to cause further expansion depends on the availability and diffusion rate of Ca^{2+} ions into the gel. None of these long cracks was observed in SMF mortar specimens.

3.1.2. Strength characteristics

For the crack propagation measurements, the maximum load required in propagating a crack in the unreinforced and SFM reinforced compact tension specimens was recorded before (at 0 days) and after the specimens were exposed to 7 and 14 days to NaOH solution. The load versus crack mouth opening displacements plots are shown in Fig. 2a and b for the unreinforced and SMF reinforced mortars, respectively. The maximum load decreased with increasing exposure time to the NaOH solution for the unreinforced mortar with the largest reduction between 0 and 7 days of exposure to the NaOH solution. However, the maximum load remained nearly constant for the SMF reinforced mortar specimens. The lack of strength degradation due to SMF supports their effectiveness in controlling cracks associated with ASR.

3.1.3. Expansion characteristics

Table 2 lists the expansion (average expansion of at least three beams) and expansion rates for the unreinforced and SMF reinforced beams. The control specimens far exceeded the expansion of the steel fiber reinforced (SFR) mortars. The SMFs are very effective in delaying the expansion and in reducing the overall expansion. The highest rate of expansion occurs during the first 2 days of exposure for the control specimens while SMF reinforced specimens showed slow initial expansion for the same period. The delay in expansion is not due to a lower permeability of the SMF mortar specimens. Permeability measurements conducted with a RbOH solution and analyzed by microprobe analysis revealed that both mortars exhibit the same permeability.

The SMFs reduce not only the initial expansion but also the overall expansion. After being exposed to the NaOH solution for up to 12 days, the SFR mortar bars expand only 33%, three times less than the control specimens. Thus, it is plausible that the difference in expansion between control and SFR mortars will increase even further with time.

3.2. Pyrex rod as reactive aggregate

3.2.1. Reactivity of Pyrex rods

The Pyrex rod in SMF mortar reacted far less compared with the unreinforced mortar at same exposure times to the NaOH solution as shown in Fig. 3. The data points were

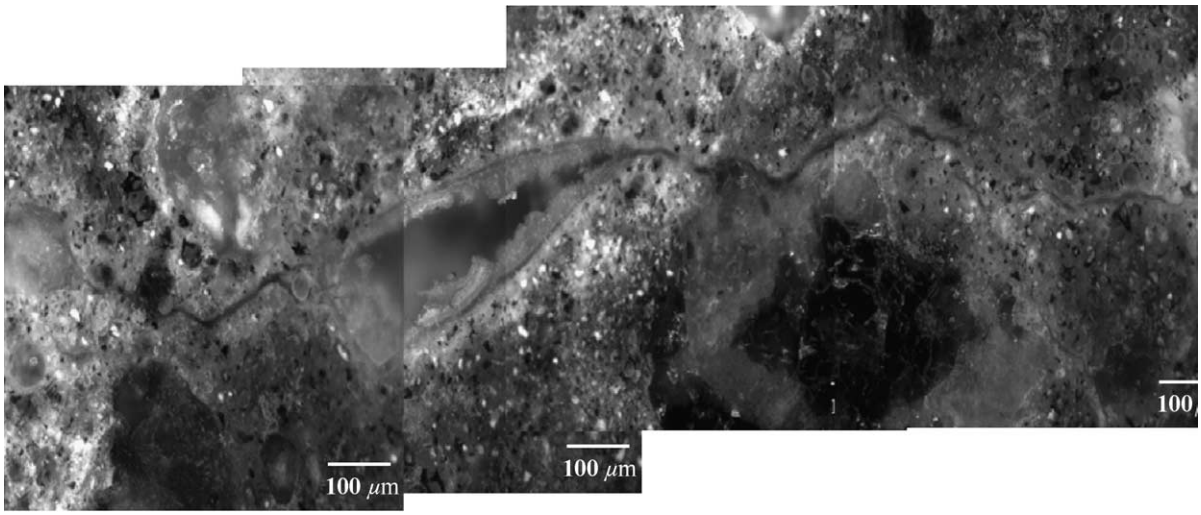

Fig. 1. Micrograph of opal aggregate exposed to 1 N NaOH solution for 32 days in control specimen; ASR rim present around opal aggregate; microcracks filled with extruded gel.

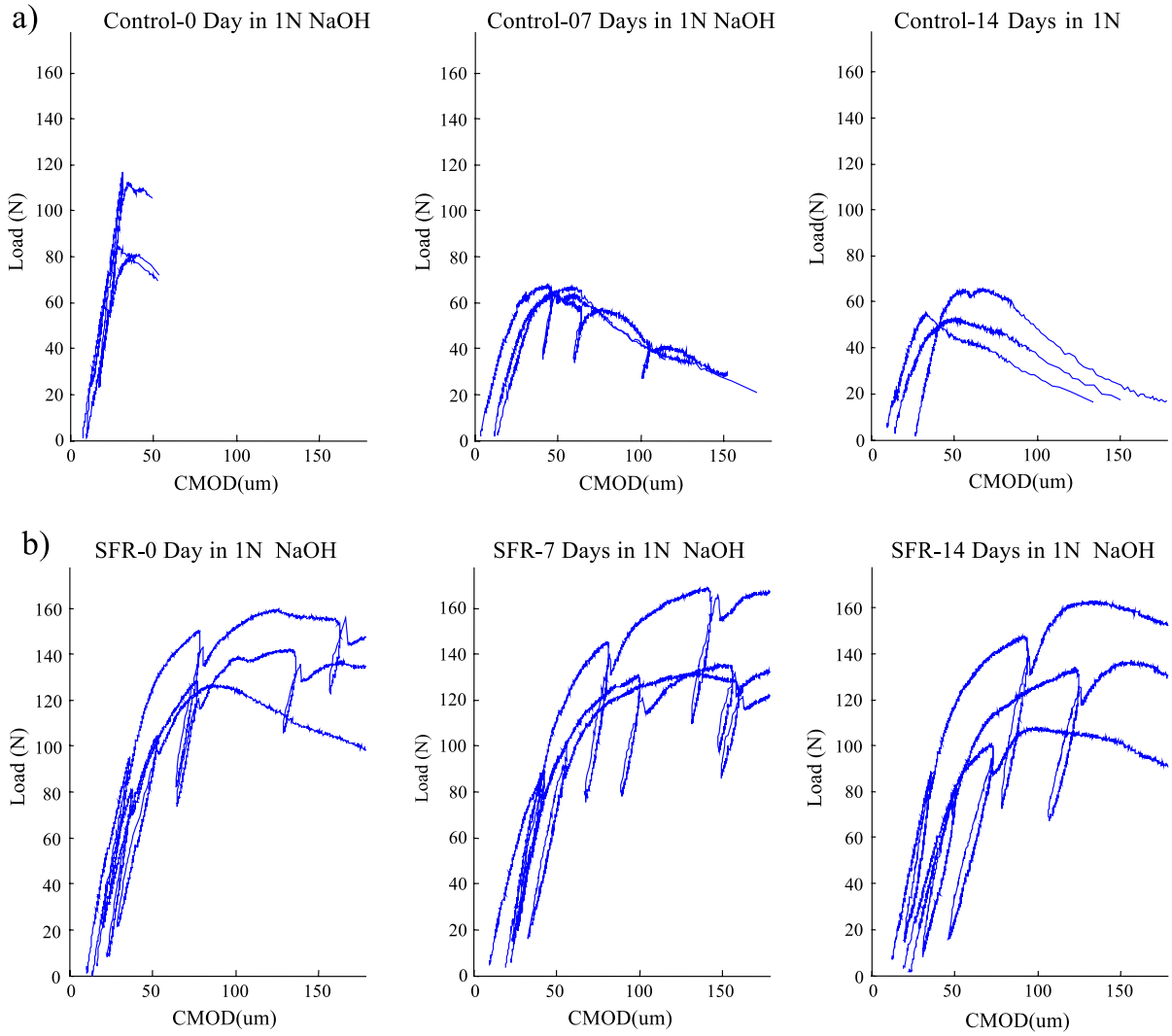

Fig. 2. (a) ASR compact tension test; load versus crack mouth opening displacements (CMOD) for control mortar specimens after exposure to 1 N NaOH solution for 0, 7 and 14 days. (b) ASR compact tension test; load versus crack mouth opening displacements (CMOD) for SMF mortar specimens after exposure to 1 N NaOH solution for 0, 7 and 14 days.

obtained from different specimens stored in 1 N NaOH solution for the desired periods. The linear best-fit lines were determined using the least squares method through the points after 7 and 14 days for the plain and SFR, respectively. The curve would eventually level off, in reality, as the continuous reaction depletes the reactants, but the abundant external source of NaOH solution in the system used for our study keeps the curve linear even after 77 days. While the curve does not depict the behavior of ASR at longer exposure times, the slope obtained from the graph gives a good indication with respect to the initial stages of the ASR where reactants are plentiful. The slopes of the curves reveal that the reaction rate is 72% faster in the control mortar. The higher reactivity of the control specimens causes the higher expansion observed (Table 2).

Table 2
Expansion data and expansion rates of control and SMF reinforced mortar prisms submerged in 1 N NaOH solution at 80 °C

Days of exposure	Expansion of control	Rate of expansion (%/day)	Expansion of 0.07 V_f	Rate of expansion (%/day)
2	0.003025	0.00151	0.000225	0.00011
6	0.004918	0.00047	0.001688	0.00037
9	0.005593	0.00023	0.001860	0.00006
12	0.006100	0.00017	0.002023	0.00005

Figs. 4 and 5 are backscattered images of the remaining cross-sections of the Pyrex rods for plain and SFR mortar specimens, respectively. All images have the same actual scanning area of 6 × 6 mm with the Pyrex rod in their center. For both specimens, the images show that the reaction takes place from the outer surface of the reactive particles and continues toward the center as reported by Powers and Steinour [20]. Note that the micrographs in Figs. 4 and 5 were taken at different exposure times to the alkali solution. The reaction is taking place evenly all

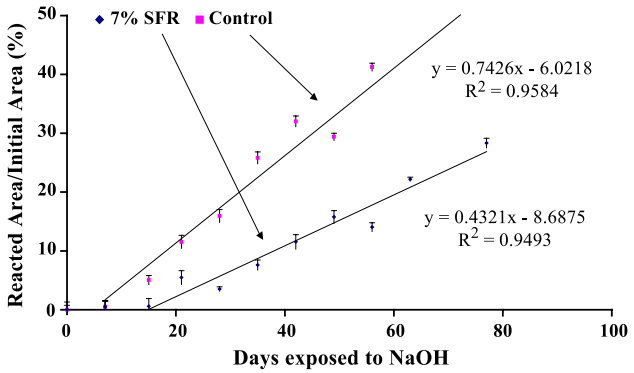

Fig. 3. Reacted area of Pyrex rod in SFR and plain mortars in NaOH (aq).

around the rod and does not seem to be modified by the presence of the voids and steel fibers located nearby.

When the specimens were cut, white precipitates and a watery liquid, presumably an alkali-silica complex, were lost resulting in a cavity between the remaining Pyrex rod and mortar. The cavity extends along the whole length of the Pyrex rod. The dark area seen around the reacted Pyrex rods (Figs. 4 and 5) is filled with epoxy used for polishing the specimen surfaces. Although most of the alkali-silica complex is lost during the preparation of the thin sections, solidified layers of gel are observed close to the mortar (Fig. 7) as will be discussed later.

Fig. 4, parts a and b, are obtained from the specimens, which had been stored in the solution for 0 and 7 days, respectively. The images revealed no visible cracks in the mortar around the rods. This observation corresponds well with the reactivity of the rod, which revealed no significant reaction before 7 days. The visible cracks, as marked with arrowheads in Fig. 4, in plain mortar surrounding the Pyrex rod are observed after 15 days of exposure to the solution. It is noted that the reactivity of the rod reaches a steady rate after 7 days as shown in Fig. 3. Thus, it seems that crack formation follows the steady rate of reaction in plain mortar bars. This suggests that the faster reactivity observed in the plain mortar bars is promoted by the formation of micro-cracks, which not only loosens the restraint around the Pyrex rod but also allows faster extrusion of silica complex out of the reaction site as will be discussed later. The images of the SMF specimens (Fig. 5) reveal no visible crack formation due to ASR even after 77 days in the 1 N NaOH solution at 80 °C.

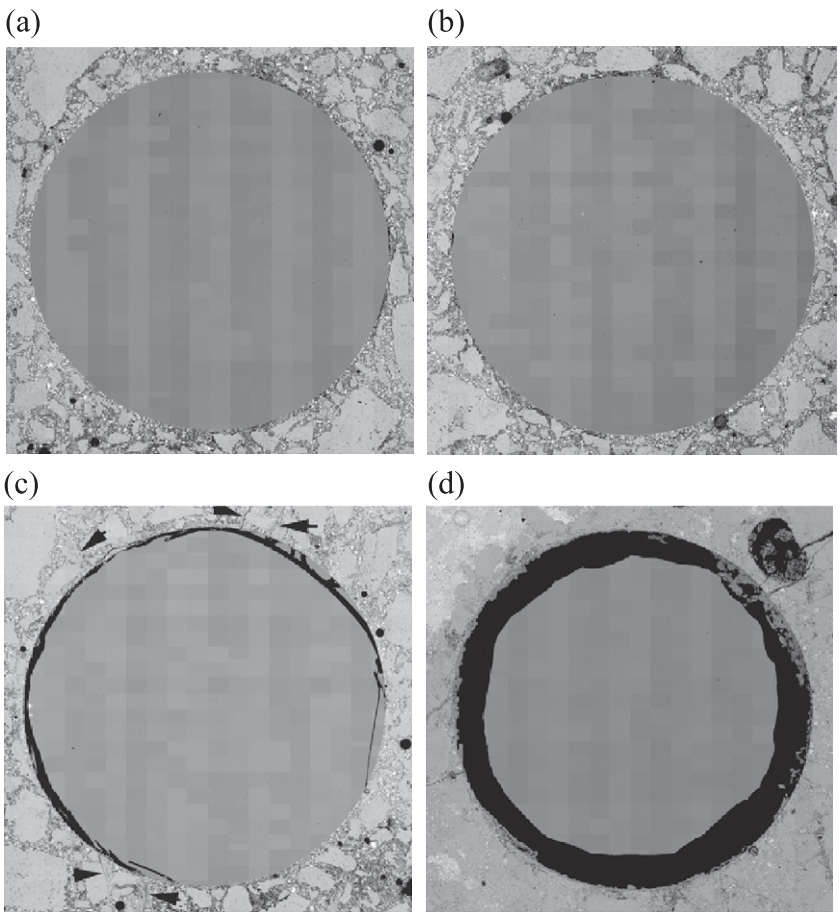

Fig. 4. Backscattered images of the remaining cross-section of Pyrex rod in plain mortar submerged in 1 N NaOH (aq) at 80 °C (actual area size of 6 × 6 mm): after (a) 0 days, (b) 7 days, (c) 15 days and (d) 42 days.

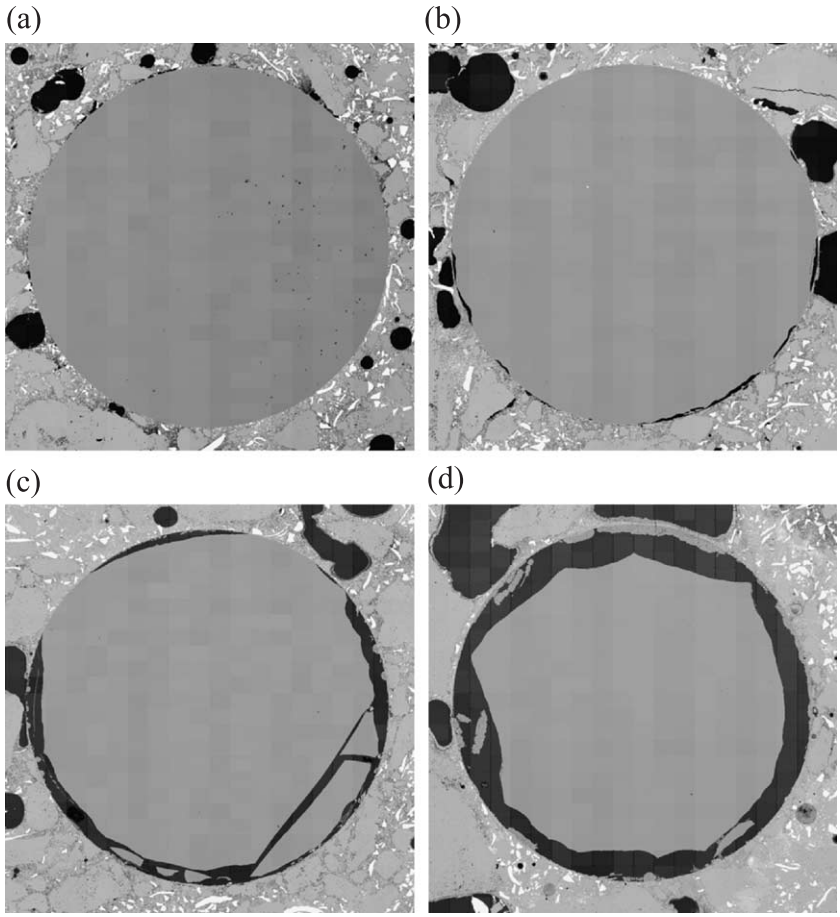

Fig. 5. Backscattered images of the remaining cross-section of Pyrex rod in SFR mortar submerged in 1 N NaOH (aq) at 80 °C (actual area size of 6 × 6 mm): after (a) 0 days, (b) 15 days, (c) 42 days and (d) 77 days. Note: Micrographs correspond to different exposure periods to alkali solution compared with Fig. 4.

3.2.2. Chemical composition of reaction products

3.2.2.1. ASR products near Pyrex-cement interface. A chemical analysis of the reaction rim was performed using the microprobe analysis. Five elements (Ca, K, Na, Si and Al) in the area were analyzed. Fig. 6 shows the typical chemical composition of ASR products near the boundary between the mortar and the Pyrex rod. The images on left in Fig. 6 are constructed by superimposing the 2D contour plots over the backscattered image, which has actual size of 300 × 186 μm. The images on the right-hand side depict the elemental content in 3D view. The Ca content of the gel ranges from 20% to 35% close to the paste and drops very rapidly away from the paste toward the rod. This gel region of high Ca content is marked as G1 in Fig. 7. The thickness of the Ca-rich gel varies from 20 to 50 μm. The amount of K in the area is insignificant compared with other elements analyzed. The wt.% of K is <1%. The highest K content is found in the G2 region forming a ridge along the boundary between G1 and G2 as shown in Fig. 6b. A sharp increase in Na content is observed toward the G2 region. The formations of Ca-rich and Na-rich gel are well-known features of the ASR gel associated with opal aggregates [20,21].

3.2.2.2. ASR products away from interface. Fig. 7 shows an empty space marked as V. This empty space had been filled with liquid alkali-silicate solution and Na-rich gel before the sample was sliced off for the sample preparation. During the preparation of the thin sections, most of the Na-rich gel and liquid were lost, and only the void space was observed under a scanning electron microscope. It is obvious that the reactivity and composition of the ASR products can be elucidated based on the concentrations of the reactants. However, there is very limited information available on the chemistry of the system directly involved with ASR in the cementitious material. Most of the published work showed the chemistry of the pore solution, which was obtained by squeezing bulk concrete or mortar subject to ASR [22]. The pore solution, therefore, lacks on information that is specific to the ASR site. Therefore, the liquid surrounding the Pyrex rod was collected and its chemical composition was analyzed by ICP spectroscopy. The Na ion concentration in the plain mortar and SMF mortar is 3.46 and 4.59 mol/l, respectively. Hence, the concentration of Na ion is much higher than that of the

external NaOH bath (≈ 1 mol/l) for both control and SFR specimens. The Si ion concentration is lower in the control specimens (2.67 vs. 3.9 mol/l in SMF mortar). Higher concentrations found in the SFR mortar can be attributed to the lack of crack formation due to SMFs. The concentrations of the other ions (i.e., Ca, K, Al, Fe and Mg) in the extract are very low compared with the Si ion concentration, ranging from 1 μmol/l to 0.003 mol/l.

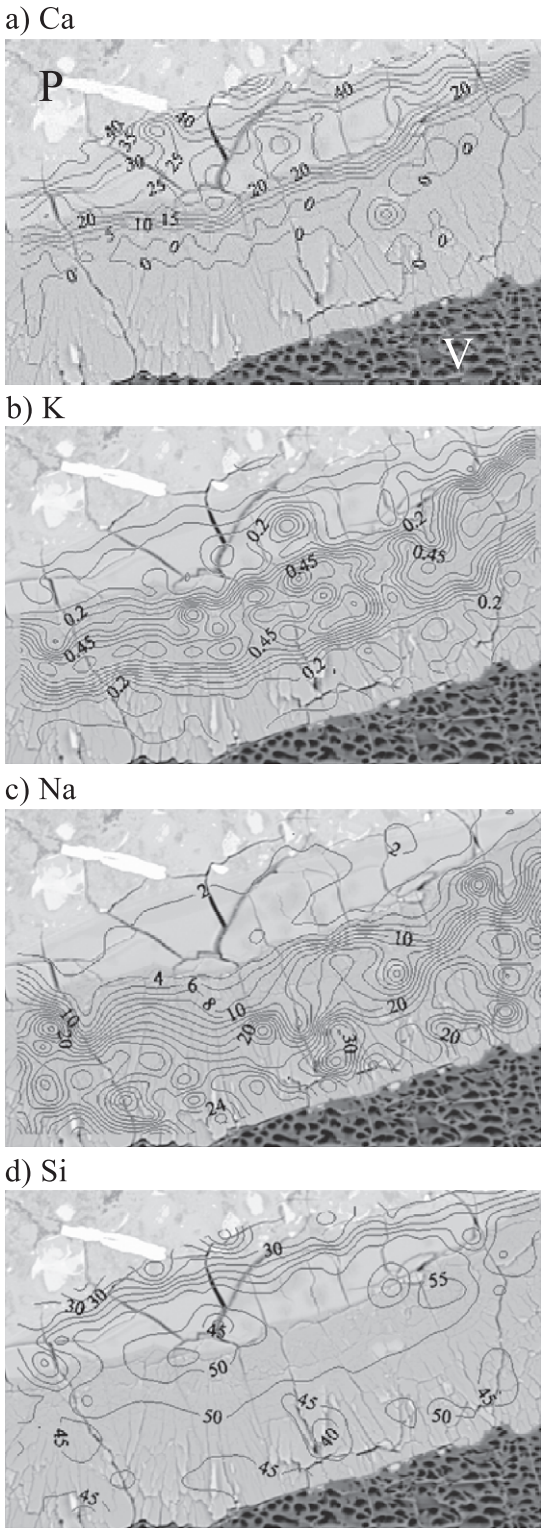

Fig. 6. Chemical analysis of reaction rim in SFR mortar (element wt.%): (a) Ca, (b) K, (c) Na and (d) Si. P, paste; V, empty space filled with epoxy.

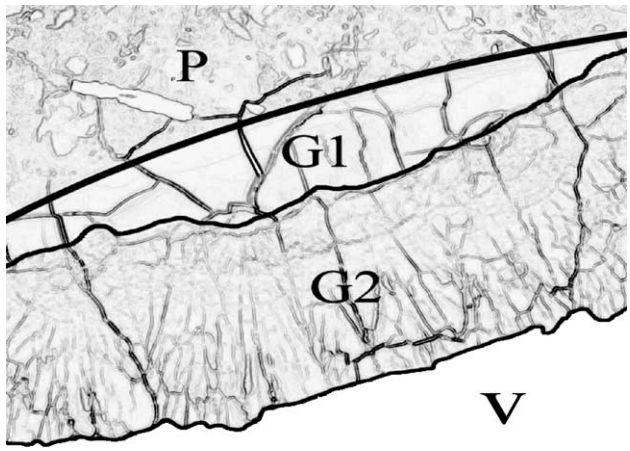

Fig. 7. Morphology of the area observed in Fig. 6: P, paste; G1 and G2, reactive product; V, void filled with epoxy containing air bubbles.

4. Discussion

SMFs are very effective in controlling cracking in mortars exposed to ASR. In both mortars with opal aggregates of various sizes and shapes and mortars with rod-shaped reactive aggregates of constant diameter, the cracking at the reactive aggregate sites were considerably reduced due to SMFs. Cracks at the reactive aggregate sites could be easily detected by optical microscopy (i.e., at low magnification) already after 7 days of exposure to the NaOH solution in control specimens with opal as reactive aggregates but not in SMF mortars. Due to crack control, the commonly observed strength loss due to ASR could be avoided. The effect of SMFs on crack control, expansion and gel formation are being addressed in the following sections.

4.1. Crack control through SMF

SMFs in cement mortars exhibit crack growth resistance behavior (Fig. 2b) due to toughening mechanisms associated with crack fiber interactions. The difference in crack growth behavior between control and SMF mortars is illustrated schematically in Fig. 8. At exposure time t_1, a crack initiates at the reactive aggregate-matrix interface in both mortar specimens. The small resistance to crack extension in the control mortar is shown by the large increase in crack length and crack opening displacement with increasing exposure time, t, to the NaOH solution. This type of crack growth behavior is characteristic of brittle materials, where the driving force for crack extension, indicated by the tensile stresses, σ, in Fig. 8a decreases

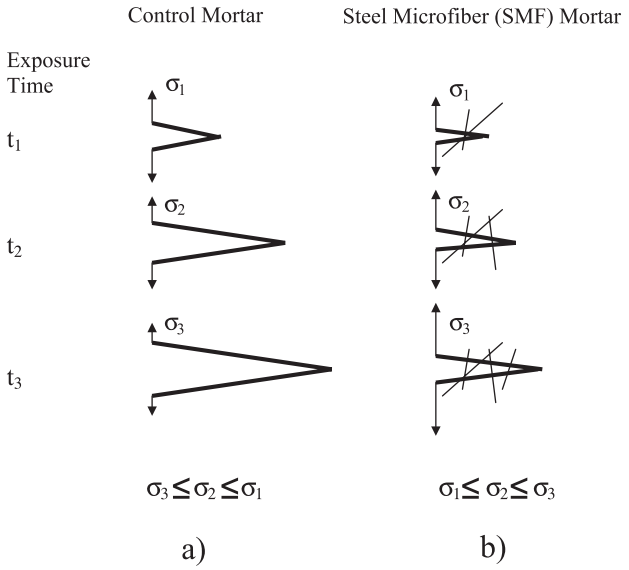

Fig. 8. Crack growth behavior due to ASR in (a) control and (b) SMF mortar specimens with increasing exposure time to 1 N NaOH solution.

with increasing crack length. The crack in the SMF mortars extends far less with increasing exposure time due to crack fiber interactions such as crack pinning, crack deflection and crack wake bridging. These energy-absorbing mechanisms increase with increasing crack length due to the formation of a bridging zone behind the crack tip. Consequently, crack extension requires the tensile stresses to increase with increasing exposure time, contrary to the control specimen (Fig. 8b).

4.2. Effect of crack growth resistance on expansion

The lack of crack growth resistance behavior in the control specimens reduces the driving force for crack extension; hence, smaller tensile stresses are sufficient to increase the crack length and the accompanying crack mouth opening displacement. Consequently, the effectiveness in constraining the expansion of the reactive aggregate decreases, as shown schematically in Fig. 9a, due to decreasing compressive stresses acting on the expanding gel with increasing exposure time. The solid circle indicates the unconstrained expansion of the reactive aggregate after exposure time t_3.

The crack growth resistance behavior in SMF mortars, which requires higher tensile stresses for crack extension, increases the effectiveness of confining the expansion of the reactive aggregate with increasing exposure time to NaOH

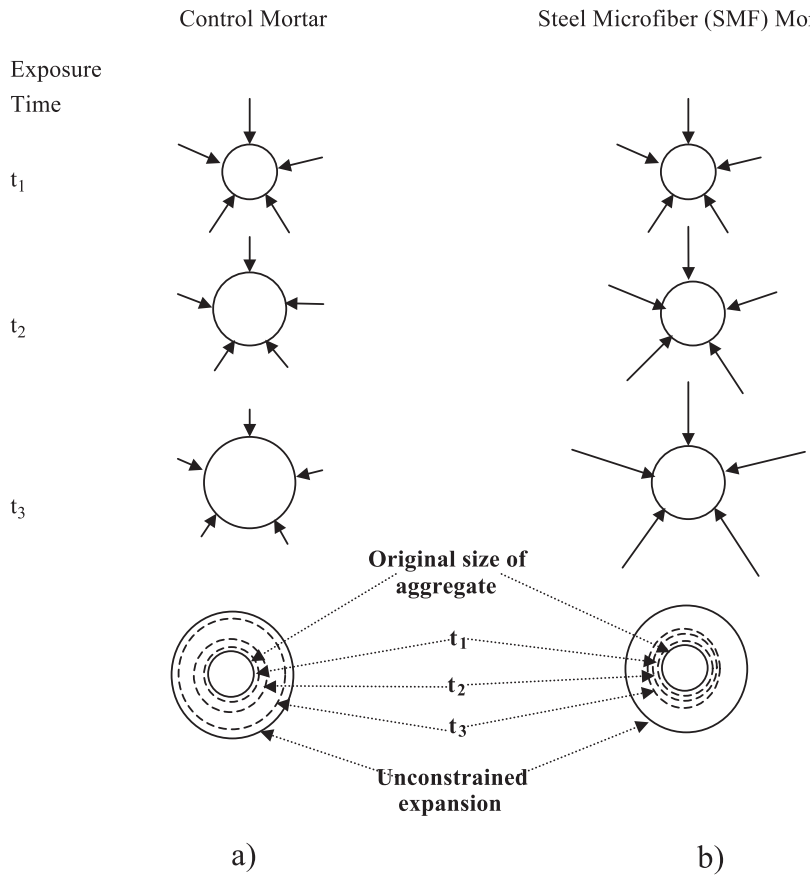

Fig. 9. Expansion characteristics of control and SMF mortar specimens due to ASR: (a) control specimen: the compressive stresses acting on the reactive aggregate decrease with increasing exposure time and (b) SMF mortar specimen: the compressive stresses increase with increasing exposure time due to crack growth resistance behavior.

solution. This increase in confinement causes an increase in compressive stresses acting on the reactive aggregate as shown in the schematic (Fig. 9b). Mitigation of expansion is hence expected and observed experimentally (Table 2).

4.3. Effect of confinement on gel formation

The combination of compressive stresses and small crack opening displacements in SMF reinforced mortar specimens not only confines the expansion of the ASR products but also limits the migration of the ASR gel away from the reaction site into the surrounding mortar matrix. Hence, the Na and Si concentration in the liquid ASR product at the reaction site has to increase as confirmed by the ICP analysis. The reduced gel formation observed in SMF mortar specimens with Pyrex rods (Fig. 5) can be explained by the increased ion concentration that suppresses further dissolution of the Pyrex rod, thereby reducing the ASR rate. The concentration of the Na ions is much higher than that of the external NaOH bath for both control and SFR specimens. Thus, this high Na concentration confirms that the NaOH solution permeates through the mortar and dissolves the Pyrex forming the alkali-silica complex. From an osmotic pressure point of view, the higher concentration of ions in the liquid ASR product is expected to exert a higher osmotic pressure in the SFR mortar compared with the plain mortar, and the smaller expansion is caused by the constraint due to SFR as discussed above. On the other hand, from the double-layer theory point of view, the higher bulk concentration found in SFR mortar would cause lower repulsive force and hence lead to smaller expansion. It is still not resolved which of the two mechanisms the alkali-silica gel uses to develop expansive forces. The formation of a reaction rim and a high concentration of the alkali-silica complex as found in the extract by ICP analysis are necessary conditions for both mechanisms.

5. Conclusion

The SMFs effectively reduce expansion associated with ASR in mortars containing crushed opal as the reactive fine aggregates by over 60% after 12 days in 1 N NaOH solution at 80 °C. The SMFs virtually eliminate the strength loss observed in unreinforced mortar specimens. Lower reactivity (i.e., less reacted area of the Pyrex rod) is observed in the SMF mortar compared with the control specimens. This low reactivity is attributed to the higher Si ion concentration found in the liquid extracted from the ASR site.

Acknowledgements

The funding for this research was provided by the National Science Foundation under grant CMS-9624980.

References

[1] N. Clayton, The effects of alkali silica reaction on the strength of prestressed concrete beams, Struct. Engr. 68 (1990) 287–292.
[2] J.K. McGowan, H.E. Vivian, Studies in cement-aggregate reaction, XXIII: The effect of superincumbent load on mortar bar expansion, Aust. J. Appl. Sci. 5 (1954) 94–97.
[3] K. Yamura, Effect of steel reinforcement on alkali silica reaction of concrete, J. Soc. Mater. Sci. Jpn. 43 (1994) 970–975.
[4] W. Koyanagi, Characteristics and simulation of concrete cracks caused by AAR, Proceedings of the 8th International Conference on Alkali Aggregate Reaction, Kyoto, 1989, pp. 845–850.
[5] T. Ahmed, E. Burley, S. Rigden, Effect of alkali-silica reaction on bearing capacity of plain and reinforced concrete, ACI Mater. J. 96 (1999) 557–570.
[6] W. Aquino, D.A. Lange, J. Olek, The influence of metakaolin and silica fume on the chemistry of alkali-silica reaction products, Cem. Concr. Compos. 23 (2001) 485–493.
[7] S. Sprung, M. Adadian, The effect of admixtures on alkali-aggregate reaction in concrete, Proceedings, Symposium on Effect of Alkalis on the Properties of Concrete, London, September. Cement and Concrete Association, Wexham Springs, Slough, 1976, pp. 125–137.
[8] R.E. Oberholster, D.M. Roy, The effectiveness of mineral admixtures in reducing expansion due to the alkali-aggregate reaction with Malmesbury group aggregates, Proceedings of the 5th International Conference on Alkali-Aggregate Reaction in Concrete, Cape Town, National Building Research Institute, Pretoria, 1981, article S252/31.
[9] M.C.G. Juenger, C.P. Ostertag, Alkali-silica reactivity of large silica fume-derived particles, *Cem. Concr. Res.*, in press.
[10] E.J. MacCoy, A.G. Caldwell, New approach to inhibiting alkali-aggregate expansion, J. Am. Concr. Inst. 22 (1951) 693–706.
[11] S. Diamond, S. Ong, The mechanisms of lithium effects on ASR, Proceedings of the 9th International Conference on Alkali Aggregate Reaction, Concrete Society of UK, London, 1992, pp. 269–278.
[12] D.W. Hobbs, Deleterious expansion of concrete due to alkali-silica reaction: influence of PFA and slag, Magn. Concr. Res. 36 (1986) 191–205.
[13] S. Diamond, Alkali silica reaction—some paradoxes, Cem. Concr. Compos. 19 (1997) 391–401.
[14] D.A. St. John, S.A. Freitag, Fifty years of investigation and control of AAR in New Zealand, Alkali-Aggregate Reaction in Concrete, Proceedings of the 10th International Conference, Melbourne, 1996, pp. 150–157.
[15] M. Kawamura, H. Fuwa, Effects of lithium salts on ASR gel composition and expansion of mortars, Cem. Concr. Res. 33 (2003) 913–919.
[16] C.K. Yi, C.P. Ostertag, Strengthening and toughening mechanisms in microfiber reinforced cementitious composites, J. Mater. Sci. 36 (2001) 1513–1522.
[17] ASTM C 1260-94, Standard test method for potential alkali reactivity of aggregates (mortar-bar method), Annual Book of ASTM Standards v. 04.02, Concrete and Aggregates, American Society for Testing and Materials, Philadelphia, 1999, pp. 650–653.
[18] L. Turanli, K. Shomglin, C.P. Ostertag, P.J.M. Monteiro, Reduction in alkali-silica expansion due to steel microfibers, Cem. Concr. Res. 31 (2001) 827–835.
[19] C.P. Ostertag, C.K. Yi, Quasi-brittle behavior of cementitious matrix composites, Mater. Sci. Eng. A278 (2000) 95–98.
[20] T.C. Powers, H.H. Steinmour, Part I—The chemical reactions and mechanisms of expansion, ACI J. 26 (1955) 497–515.
[21] R.F. Bleszynski, M.D.A. Thomas, Microstructural studies of alkali-silica reaction in fly ash concrete immersed in alkaline solution, Adv. Cem. Based Mater. 7 (1998) 66–78.
[22] B. Durand, J. Berard, R. Roux, J.A. Soles, Alkali-silica reaction: the relation between pore solution characteristics and expansion test results, Cem. Concr. Res. 20 (1990) 419–428.